J. Fluid Mech. (1998), *vol.* 366, *pp.* 333–350. Printed in the United Kingdom

On large-amplitude pulsating fountains

By CHRISTOPHE CLANET†

Department of Applied Mechanics and Engineering Sciences, University of California San Diego, La Jolla, CA 92093–0411, USA

(Received 6 January 1997 and in revised form 17 February 1998)

We study the behaviour of an upward vertical water jet of density, ρ, and surface tension, σ, injected through a tube of diameter, D, with a momentum-averaged velocity, V. These fountains are shown to exhibit large-amplitude oscillations in the range $0.1 \leqslant D/a \leqslant 1.6$, and $20 \leqslant V^2/(gD) \leqslant 400$, where g is the acceleration due to gravity and a is the capillary length, $a \equiv (2\sigma/(\rho g))^{1/2}$. The characteristic frequency of the oscillations, f, and their limits of existence are studied experimentally. A model is developed, leading to the expression for the frequency:

$$f = \frac{g}{3V}.$$

This expression is shown to be in good agreement with existing data and with new measurements, conducted over a wide range of Bond ($Bo \equiv D/a$) and Froude ($Fr \equiv V^2/gD$) numbers. The stability of the model is considered and the limits of the oscillatory regime are related to the hydrodynamic properties of the flow.

1. Introduction

Greek mythology considers fountains as the place where *Naiads*‡ play. We follow this tradition and try to prove that these *Nymphs* are not responsible for the oscillations of some of the fountains we encountered . . . .

The water fountains we consider point vertically upwards and are characterized by an internal diameter D, and an outer diameter D_o. The fluid of density, ρ, and surface tension, σ, is ejected with a momentum-averaged velocity V, as presented in figure 1(*a*).

Depending on the initial momentum flux ($\sim \rho V^2$), these fountains are known to exhibit several modes of behaviour (Schulkes 1993). For very low-momentum fluxes, the water exiting the fountain remains attached to the nozzle due to capillary and gravity forces (figure 1*b*). This first regime has been studied by Dias & Vanden-Broeck (1990). For values of the momentum flux above a certain threshold, a second regime is achieved where the fluid detaches from the nozzle, forming an upward moving jet. The upward moving fluid then changes kinetic into potential energy until it reaches a maximum height at which point a lump of fluid begins to accumulate at the tip of the fountain. As the mass of the lump increases, the pull of gravity

† Present address: Institut de Recherche sur les Phénomènes Hors Equilibre, Université de Provence, centre de St. Jérôme, service 252, Marseille Cedex 20, France.

‡ From Greek naiein, 'to flow': one of the nymphs of flowing water springs, rivers, fountains, lakes. The Naiads, appropriately because of their relation to freshwater, were represented as beautiful, lighthearted, and beneficent. Like the other classes of nymphs, they were extremely long-lived, although not immortal.

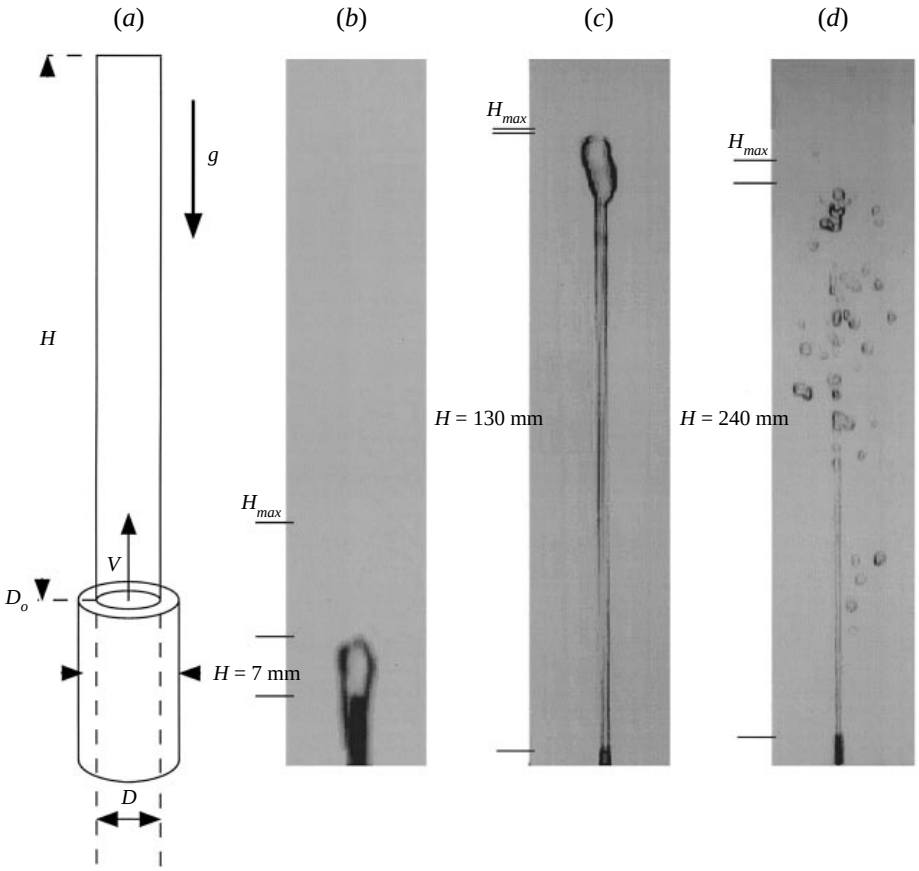

FIGURE 1. (*a*) Sketch of the fountain, (*b*) lower limit, $D = 1.194$ mm and $V = 0.63$ m s^{-1}, (*c*) Oscillating regime, $D = 1.194$ mm and $V = 1.61$ m s^{-1}, (*d*) Upper limit, $D = 1.194$ mm and $V = 2.21$ m s^{-1}.

eventually overcomes the jet's momentum and the lump begins to fall (figure 1*c*). As the falling lump reaches the nozzle, it dislodges from the jet and a new cycle begins. This rising and falling process repeats itself in a periodic or quasi-periodic fashion resulting in large-amplitude oscillations in the fountain's height as shown in figure 2. As the water momentum is further increased, this oscillatory behaviour persists at increasing amplitudes until a second threshold limit is reached above which the fountain no longer exhibits high-amplitude pulsations (figure 1*d*). In the case of water fountains, the intermediate, large-amplitude oscillatory regime exists within the limits $0.1 \leqslant D/a \leqslant 1.6$ and $20 \leqslant V^2/gD \leqslant 400$, where g is the acceleration due to gravity and a is the capillary length, $a \equiv (2\sigma/(\rho g))^{1/2}$.

Over the years, several studies have dealt with large-amplitude oscillating fountains (Villermaux 1994) and plumes (Priestley 1953; Turner 1966). In the case of fountains, Villermaux shows *that a vertical water jet undergoes self-sustained pulsations in height, associated with the gravity-induced backflow of the jet on itself*. He then uses the diameter, D, of the jet as the characteristic length involved in the backflow process and proposes the use of a delay time $\tau_d \sim (D/g)^{1/2}$ to implement the nonlinear delayed saturation (NLDS) model of Villermaux & Hopfinger (1993) to evaluate the period of the oscillations. However, in the NLDS model ($\mathrm{d}A/\mathrm{d}t = rA(t) - \mu|A(t-\tau_d)|^2 A(t)$), the

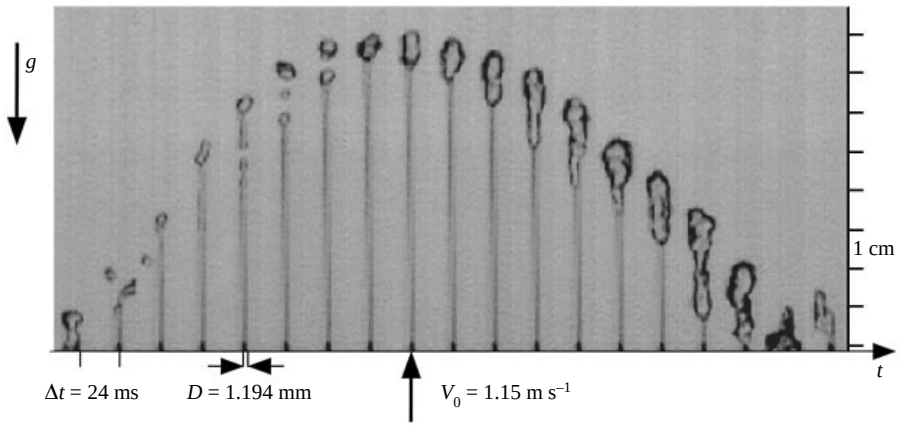

FIGURE 2. Large amplitude pulsating mode of a water fountain, $D = 1.194$ mm and $V = 1.33$ m s^{-1}.

period of the oscillations depends on the parameters r, μ and τ_d. Villermaux (1994) chooses the delay, τ_d, but does not specify r and μ, which prevents the determination of the period of the oscillations. In this sense, the model he proposes is not complete and no comparison can be made with our contribution.

Here, we will show that the period of the oscillations does not depend on the diameter of the jet, but rather scales as $T \sim (H_{max}/g)^{1/2}$, where H_{max} is the maximum height reached by the fountain ($H_{max} = V^2/2g$).

The same scaling was obtained by Turner (1966), considering the oscillations of plumes which are initially buoyant and become heavy as they mix with the environment. This system also exhibits large-amplitude pulsations (of the order of the maximum height) with a characteristic period τ related to the maximum height z_{max} of the plume by the relation $\tau = C(z_{max}/\Delta_2)^{1/2}$, where Δ_2 is a reduced gravity and C is a constant that was evaluated experimentally and found to be close to 14. In the case of fountains, the same dimensional analysis can be made in which case Δ_2 reduces to g so that $\tau \sim (z_{max}/g)^{1/2}$.

This paper addresses issues concerning the physics of the oscillations, the evolution of their characteristic frequency and their limits of existence. Physical models are developed and compared with existing experimental data and with new measurements, performed over a wide range of jet diameters and velocities. Section 2 presents the experimental set-up and the range of variation of the control parameters. Section 3 is dedicated to the presentation of the experimental results and § 4 to the model. The validity and stability of the model are discussed in § 5 and the limits of the pulsating regime in § 6.

2. Experimental set-up

All the reported experiments were performed using deionized water at room temperature (22°C), the properties of which are recalled in table 1, where ν is the kinematic viscosity. Deionized water was supplied to the fountain's nozzle at a constant pressure through a regulator and flowmeter. The nozzles consisted of cylindrical, stainless steel hypodermic needles with inner diameter, D, outer diameter D_o, and length/diameter ratios $L/D > 50$. In our experiment, the external diameter, D_o, is not varied independently of D but is fixed by the thickness of the material used to make the needles. The relation between D_o and D can be well approximated by the third-order polynomial

ρ(kg m^{-3})	v(m^2 s^{-1})	σ(kg s^{-2})	a(m)
1000	10^{-6}	0.073	3.8×10^{-3}

TABLE 1. Physical properties of dionized water at 22°C.

$D_o = M_0 + M_1 D + M_2 D^2 + M_3 D^3$ with $M_0 = 4.16 \times 10^{-5}$, $M_1 = 1.83$, $M_2 = -501$ and $M_3 = 1.01 \times 10^5$. The control parameters of the experiments are the nozzle inner diameter D, and the jet mean exit velocity V_0 defined as the ratio of the mean exit flow rate to the exit cross-section area. The mean exit flow rate was measured with an accurate rotameter (130 units corresponding to 19.3 cm^3). The exit velocity profile was estimated assuming a fully developed pipe flow so that, as shown in Appendix A, the momentum-averaged velocity, V, is equal to $2/\sqrt{3}V_0$ for a laminar jet and very close to V_0 for a turbulent one. The Reynolds number Re, for transition from laminar to turbulent flow was determined for each needle using tilting (see Appendix A) and was found to vary from $Re \approx 2500$ to $Re \approx 4000$, where $Re \equiv V_0 D/v$. The range of variation of the parameters D, D_o and V_0 is reported in table 2, where subindex 1 corresponds to the lowest threshold of oscillation, and 2 to the upper one. The corresponding Reynolds numbers are also presented in table 2. The transition values, V_{01} and V_{02}, between the oscillating regime and the non-oscillating one, are determined experimentally with an accuracy of 20%, corresponding to the repeatability of the measurements. For the smallest diameters used ($D = 0.318$ and 0.394 mm), as soon as the jet detaches from the nozzle we always observed an umbrella-like fountain without any oscillating regime in between (figure 1*d*). Thus, we only report the velocity V_{01} in the table. For the next two diameters ($D = 0.495$ and 0.584 mm), the difference between V_{01} and V_{02} corresponds to less than one graduation on the rotameter; therefore, no systematic study of the evolution of the frequency was done in these cases. For these diameters, V_{01} and V_{02} were determined by weighting and timing the outflowing water. For all other cases, the time evolution of the fountain's height was recorded using a high-speed video camera *Ektapro-1000*. Digital image processing was applied to the recorded data using the *NIH image 1.60* image processing package and *Matlab*. A threshold method was applied to obtain a binary image, the background corresponding to 0 and the water jet to 1. Defining a window that was approximately two diameters wide and more than 1.5 H_{max} long, the Matlab program projected the matrix corresponding to this window onto a line, and determined the height of the fountain as the location of the furthest 1 value found. This method does not assume continuity of the jet. The instantaneous height of the fountain is defined as the location of the highest particle of water on the axis. The framing rate was always adjusted to ensure an accurate resolution of the frequencies of interest (typically 20 frames per period). Between 1024 and 2048 images were recorded for each condition, and the resulting $H(t)$ file was then processed with *Matlab*, using a fast Fourier transform routine.

3. Experimental results

An example of the time evolution of the height of the fountain, $H(t)$, is presented in figure 3, corresponding to the same conditions as the visualization sequence shown in figure 2. One notices that the maximum height, $H_{max} = V^2/2g \approx 9$ cm, is rarely reached, which means that some energy losses prevent the initial kinetic energy

D (mm)	D_o (mm)	V_{01} (m s^{-1})	V_{02} (m s^{-1})	Re_1	Re_2
0.318	0.635	1.28	—	407	—
0.394	0.711	0.79	—	311	—
0.495	0.813	0.77	1.2	381	594
0.584	0.902	0.71	1.3	414	759
0.838	1.27	0.63	1.5	527	1257
1.19	1.65	0.60	1.9	714	2261
1.60	2.11	0.61	2.1	976	3360
2.16	2.77	0.60	2.7	1290	5832
3.2	4.0	0.76	2.6	2432	8320
4.1	6.1	0.9	2.3	3690	9430

TABLE 2. Range of variation of the different relevant parameters.

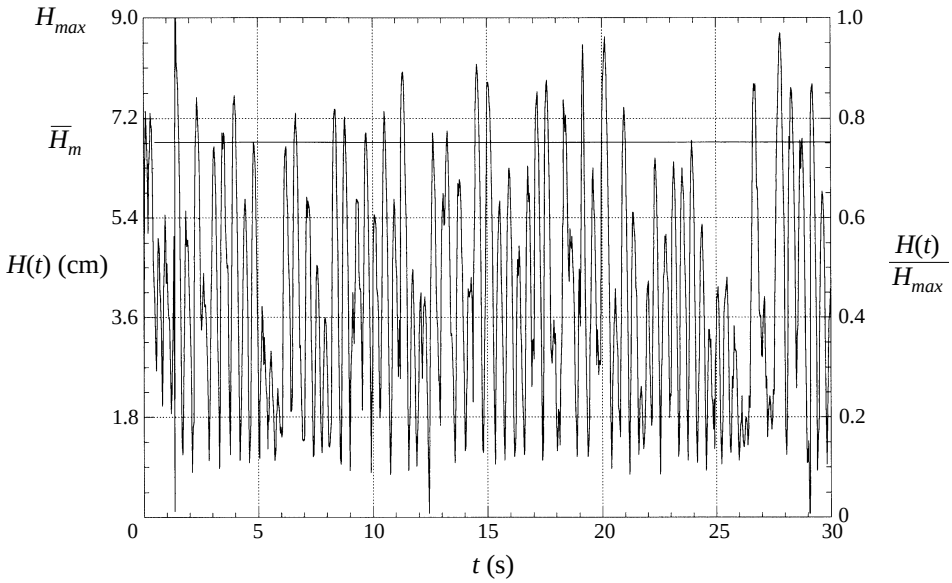

FIGURE 3. Time evolution of the fountain's height, $D = 1.194$ mm and $V = 1.33$ m s^{-1}.

being fully converted in potential energy. To quantify this effect, we define a mean maximum height, $\overline{H_m}$, which is also presented in figure 3. These losses are considered in more detail in § 5. In each case, the characteristic frequency of the pulsation was measured from the power spectrum of these measurements. The corresponding Fourier transform of the time evolution presented in figure 3 is shown in figure 4. Note that the Fourier transform exhibits a clear peak, indicating that in this case, the characteristic frequency of the pulsation is 2.3 Hz. This frequency, f, was found to monotonically decrease as V was increased (figure 5).

Furthermore, in the whole velocity range, the frequency appears to be independent of the nozzle diameter, D, that was varied by a factor of 5. Close to the lower and upper limits of the pulsating regime, the measured noise that can be noticed in figure 4 becomes of the same order as the signal itself and no characteristic frequency could be measured.

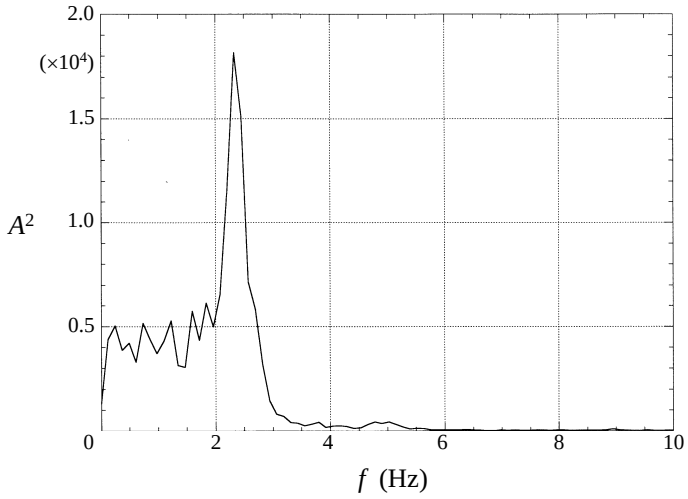

FIGURE 4. Fourier transform of the fountain's height signal obtained with $D = 1.194$ mm and $V = 1.33$ m s^{-1}.

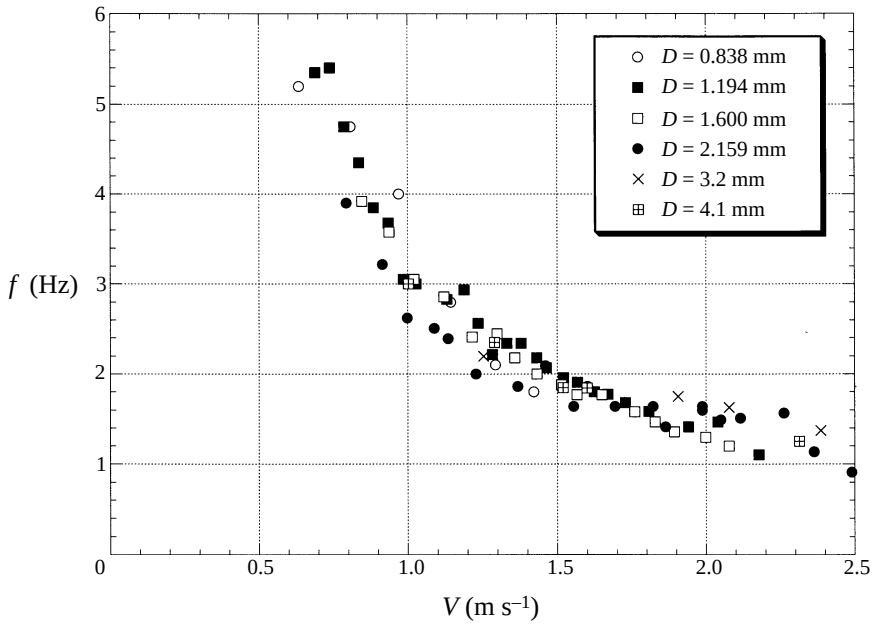

FIGURE 5. Evolution of the characteristic frequency with the velocity V for different diameters D.

4. The model

In the ascending portion of the cycle, we consider that the upward moving fluid loses its momentum because of gravity until it reaches a maximum height, H_{max}. Then, under the combined effect of gravity and of the momentum flux provided by the jet, a fluid lump of mass, M, forms at the tip and begins to fall with a velocity U (figure 6). When the falling liquid lump reaches the nozzle, it dislodges from it, and a new oscillation cycle begins.

Assuming that at the end of the descending portion of the pulsation the entire

mass of the lump instantaneously detaches from the nozzle, the ascending jet is simply described by the conservation of mass and energy. Thus, $v(z)s(z) = VS_0$, and $\rho V^2 = \rho v^2(z) + 2\rho gz$, where $v(z)$ and $s(z)$ are respectively the velocity and cross-sectional area of the jet at the z-location. Correspondingly, V is the exit characteristic velocity and $S_0 \equiv \pi D^2/4$ the exit cross-section. The conservation of energy takes the form

$$\frac{v(z)}{V} = \left(1 - \frac{2gz}{V^2}\right)^{1/2}. \tag{4.1}$$

Equation (4.1) gives the velocity v of the jet at each z-location, from $z = 0$ where $v = V$ to $z = H_{max} = V^2/2g$ where $v = 0$. Considering the dynamics of the lump as shown in figure 6, the conservation of mass and momentum, applied to the lump, leads to

$$\frac{\mathrm{d}M}{\mathrm{d}t} = \rho s(z)\,[v(z) - U(z)] \tag{4.2}$$

and

$$\frac{\mathrm{d}(MU)}{\mathrm{d}t} = -Mg + \rho s(z)v(z)\,[v(z) - U(z)] \tag{4.3}$$

where $M = U = 0$ at $z = H_{max}$. Transforming the time derivative into a space one with the relation $U = \mathrm{d}z/\mathrm{d}t$ and introducing dimensionless variables $z^* = z/H_{max}$, $t^* = tV/(4H_{max})$, $U^* = 4U/V$, and $M^* = M/(\rho S_0 H_{max})$, one gets the following forms for the conservation of mass and momentum:

$$\frac{\mathrm{d}M}{\mathrm{d}z} = 4\frac{v - U}{Uv} \tag{4.4}$$

and

$$U\frac{\mathrm{d}(MU)}{\mathrm{d}z} = -8M + 4(v - U). \tag{4.5}$$

The velocity of the jet, given by equation (4.1), is reduced to

$$v = 4(1 - z)^{1/2}. \tag{4.6}$$

For simplicity, in equations (4.4), (4.5) and (4.6), we have dropped the asterisks in the notation of the dimensionless variables. The unknowns being $U(z)$ and $M(z)$, the system (4.4) and (4.5) with (4.6) must satisfy the conditions $U(1) = v(1) = M(1) = 0$. This system can be solved exactly, making the guess that U and M depend on z through the same function as v, that is $U(z) = av(z)$ and $M(z) = bv(z)$ with a and b constants. This assumption satisfies the limit conditions since $v(1) = 0$. The two constants a and b are determined using the equations (4.4) and (4.5):

$$b = -\frac{1}{2}\left(\frac{1 - a}{a}\right) \tag{4.7}$$

and

$$2a^2 - a - 1 = 0 \Rightarrow \begin{cases} a_1 = 1 \\ a_2 = -\frac{1}{2}. \end{cases} \tag{4.8}$$

The first solution ($a_1 = 1, b_1 = 0$) describes the evolution of the lump during the ascending phase. All the fluid of the lump from the previous cycle has been shed and the new cycle starts with an empty lump ($M = 0$) that rises with the same velocity as the jet ($U = v$). This first solution applies until $z = 1$. The second solution ($a_2 = -1/2, b_1 = 3/2$) describes the descending part of the cycle.

Concerning the mass of the lump, we conclude that at the end of the descending

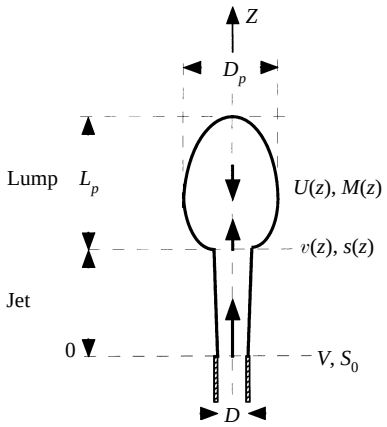

FIGURE 6. Model for the interaction.

phase, $M(0) = 6$ since $v = 4$ and $M = bv$. In dimensional form, this means that the mass of the lump at the point where it dislodges from the nozzle is $M = 6\rho S_0 H_{max}$.

The above solution shows that, on the way down, the velocity of the lump at each z-location is half the velocity of the ascending jet at the same location. In other words, it takes twice as long for the lump to fall down as it took the fluid element to rise from the nozzle to the tip of the fountain. Therefore, the total period, T, of the oscillation is three times the ascending time T_a. Using $U = v$ for the ascending phase, one gets

$$T_a = \int_0^1 \frac{\mathrm{d}z}{v(z)} = \frac{1}{2}. \tag{4.9}$$

The period of the pulsation is then $T = 3/2$. Expressing the *effect* (the oscillation) with a Strouhal number, $St \equiv fD/V$, and the *cause* (gravity) with a Froude number, $Fr \equiv V^2/gD$, the oscillation satisfies

$$St = \tfrac{1}{3} Fr^{-1}. \tag{4.10}$$

This linear dependency is plotted in figure 7, and is compared to the experimental results. Observe that the measured Strouhal numbers are in good quantitative agreement with the model. The estimated error in the measurements is approximately 15%, according to their repeatability.

In Villermaux (1994), the reported experiment is conducted using tap water with a converging nozzle of exit diameter, $D = 3$ mm, and a mass-averaged velocity $V_0 = 1.5$ m s^{-1}. According to the author, the oscillation frequency is about 2 Hz. The model presented above can be tested on this set of data, which is the only one we found in the literature. The jet Reynolds number being $Re = 4500$, we assume the jet to be laminar and obtain the momentum-averaged velocity $V = 1.73$ m s^{-1}, which leads to $f = g/(3V) = 1.9$ Hz (for a turbulent jet, $V = 1.5$ m s^{-1}, one gets $f = 2.2$ Hz). This is consistent with Villermaux' observations.

5. Validity and stability of the model

The model we propose assumes a 'perfect cycle', in the sense that the fluid always reach H_{max}, that the lump does not break until it reaches the nozzle and dislodges from it instantaneously, prior to the new cycle. These assumptions are to be tested in

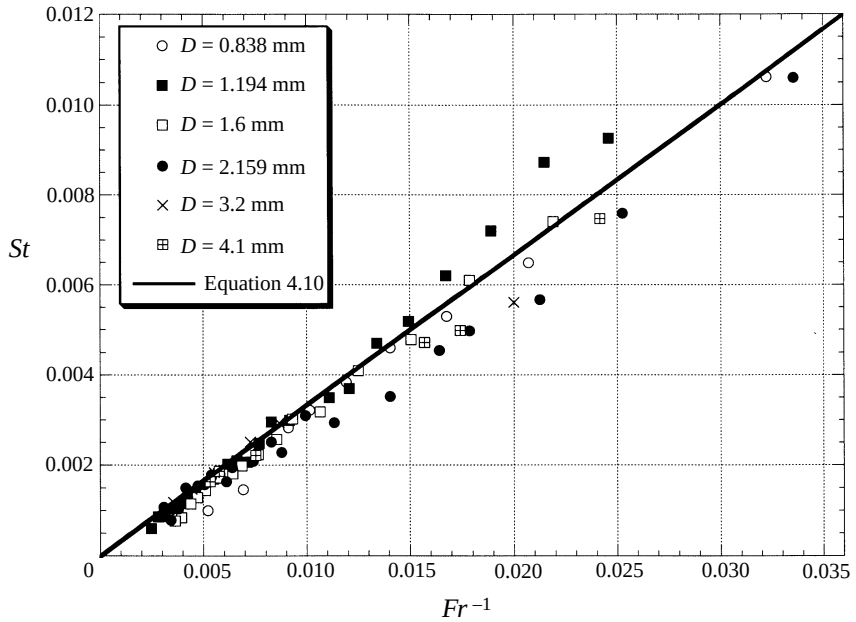

FIGURE 7. Comparison between the model and the experimental data obtained with different diameters.

this section as well as the mechanism by which the jet communicates momentum to the lump.

It was assumed that the momentum of the jet is transmitted to the whole lump instantaneously so that the lump behaves like a 'solid body'. In other words, a model with interacting solid spheres, such as a one-dimensional juggler, should lead to the same result, as far as the period of the oscillation is concerned (see Appendix B). To analyse the validity of this assumption, let us estimate the order of magnitude of the time required to exchange momentum between the jet and the lump. Consider a lump characterized by its length L_p and its width D_p (figure 6). In a reference frame stationary with respect to the lump, the jet enters the lump with a velocity, $V_j = v(z) - U(z)$, and a diameter $D_j = (4s(z)/\pi)^{1/2}$, respectively of the order of V and D. As the jet discharges into the lump, the momentum of the jet, $\rho V_j^2 D_j^2 \sim \rho V^2 D^2$, is transferred to the fluid inside the lump, inducing a turbulent motion with mean axial velocity V_p:

$$\rho V_p^2 D_p^2 \sim \rho V^2 D^2 \text{ or equivalently} \frac{V_p}{V} \sim \frac{D}{D_p}. \tag{5.1}$$

The lateral transfer of momentum over the distance D_p occurs in a characteristic time $T_d \sim (D_p)^2/v_t$, where v_t is the turbulent kinematic viscosity. We estimate $v_t \sim \alpha V_p D_p$ where α is a constant smaller than 1, Landau & Lifchitz (1971). The characteristic time of interaction of the jet with the lump can be estimated as $T_i \sim L_p/V_p$. If the two times T_i and T_d are of the same order of magnitude, the momentum from the jet is transmitted to the whole lump during the interaction. According to the previous estimates, this condition can be written as

$$\frac{L_p}{V_p} \sim \frac{D_p^2}{\alpha V_p D_p} \quad \text{or equivalently} \quad \frac{L_p}{D_p} \sim \frac{1}{\alpha}. \tag{5.2}$$

From pictures (figure 2), $1/\alpha$ is estimated to be between 3 or 4. The length of the lump is evaluated, requiring that the induced kinetic energy in the lump ρV_p^2 is converted into potential energy over its length L_p, resulting in

$$\rho g L_p \sim \rho V_p^2 \quad \text{or equivalently} \quad \frac{D_p}{D} \sim \left(\alpha \frac{V^2}{gD}\right)^{1/3}. \tag{5.3}$$

In the experiment presented in figure 2, the Froude number is of the order of 150, which leads to $D_p/D \sim 3.5$. This estimation is in good qualitative agreement with the experiments.

Finally, using equations (5.2) and (5.3), the mass of the lump, $M \sim \rho D_p^2 L_p$, is evaluated as

$$M \sim \rho D^3 \frac{V^2}{gD} \quad \text{or} \quad M \sim \rho D^2 H_{max}. \tag{5.4}$$

This relation has the same form as the one obtained from the model ($M = 6\rho S_0 H_{max}$). We then conclude that the order of magnitude analysis is consistent with the assumption that the transfer of momentum to the whole lump is done during the time of the interaction.

We now consider the stability of the model regarding the energy losses that occur, for example, during the shedding of the lump at the end of a cycle or when a small amount of liquid is transported into a new cycle (figure 2, where during the ascending phase, some of the liquid from the previous cycle remains). If $1/2\rho V^2 \epsilon$ represents this energy loss, the energy balance leads to a new expression for $v(z)$:

$$\frac{v(z)}{V} = \left(1 - \frac{2gz}{V^2} - \epsilon\right)^{1/2}. \tag{5.5}$$

This expression is analogous to equation (4.1) and both are the same for $\epsilon = 0$. This loss of energy alters the maximum height, H_m, reached by the jet which can be compared to H_{max}, obtained without losses:

$$H_m = \frac{V^2}{2g}(1 - \epsilon) \text{ or } \frac{H_m}{H_{max}} = (1 - \epsilon). \tag{5.6}$$

The value of ϵ can be evaluated experimentally from figure 8, where we present the mean maximum height, $\overline{H_m}$, as a function of the maximum height, H_{max}, for different nozzle diameters. From this figure, we get $\epsilon \approx 0.24$, which means that about 24% of the initial energy is lost, whether in the shedding process or in the transport of a recirculating mass.

Focusing on the dynamics of the lump, equations (4.2) and (4.3) remain unchanged. Furthermore, using the same parameters for the non-dimensionalization of the system, we get the same system as (4.4) and (4.5) with just a new expression for the jet velocity at each z location:

$$v(z) = 4(H_m - z)^{1/2}. \tag{5.7}$$

In this expression, the asterisks have been omitted for simplicity. Making the same assumptions, $U(z) = av(z)$ and $M(z) = bv(z)$, it follows that equations (4.7) and (4.8) still hold, so that the final period, T, is three times the rising time, T_a defined as:

$$T_a = \int_0^{H_m} \frac{\mathrm{d}z}{v(z)} = \frac{H_m^{1/2}}{2} \approx \tfrac{1}{2}\left(1 - \epsilon/2\right) \tag{5.8}$$

which shows that the effect of the energy loss is to change the period of the oscillation

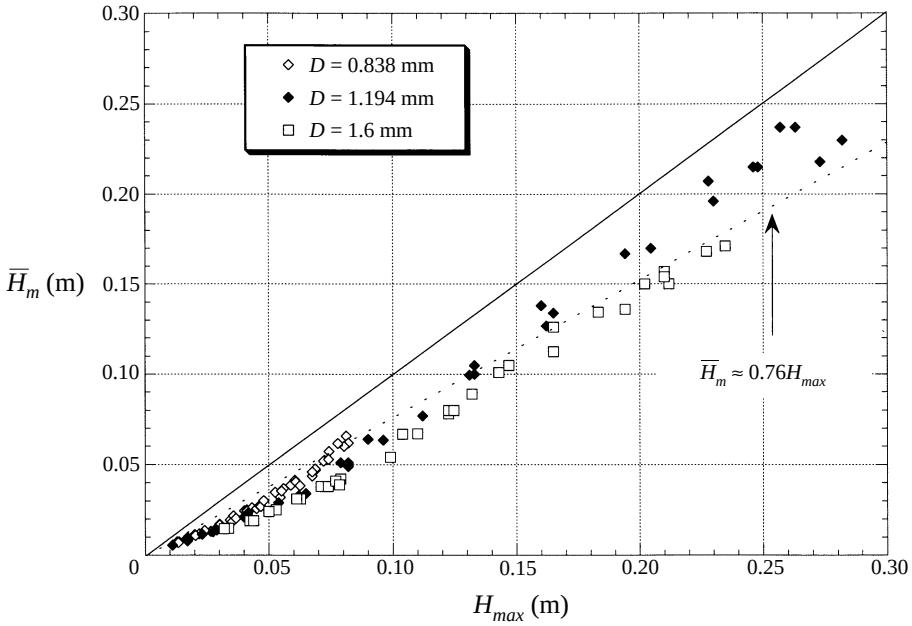

FIGURE 8. Mean maximum height as a function of the maximum height.

by a factor $\epsilon/2$. According to the previous estimation of ϵ, the period should be 12% shorter than the one calculated with the no-energy-loss model.

Furthermore, the interaction of the lump with the nozzle at the end of each cycle occurs in a characteristic time $T_i \sim 2L_p/V$ that has been considered, in the model, to be small compared to the period $T \sim 3V/g$. Using the evaluations (5.2) and (5.3) for L_p and D_p, we get:

$$\frac{T_i}{T} \sim \frac{2}{3}\left(\frac{1}{\alpha}\frac{gD}{V^2}\right)^{2/3}. \tag{5.9}$$

For a typical value $Fr = 100$, we get $T_i/T \approx 0.07$. Thus this effect could increase the estimated period of the oscillation by as much as 7%.

To conclude this section on the stability of the model, it is of interest to note that the energy loss tends to decrease the total period but the time it takes for this energy loss to happen tends to increase it. The two effects being of the same order of magnitude, it is reasonable to conclude that the model is stable, and that the 'perfect cycle' period is a good evaluation of the real period of the oscillations.

6. Limits of the pulsating regime

In this section we identify the physics of the *lower* and *upper* velocity thresholds of the pulsating mode.

In the lower range, a spherical bulb forms at the nozzle exit and remains 'attached' to it due to both capillary and gravity forces (figure 1*b*). The pulsating mode starts once the jet momentum flux is high enough to overcome these two forces. The capillary action is of the order $\pi\sigma D_o$. From experimental observations, the characteristic diameter of the bulb is of the order of $2D_o$, and its weight can be estimated as $4/3\pi D_o^3\rho g$. The threshold velocity is then given by $\rho\pi D^2V^2/4 = 4/3\pi D_o^3\rho g + \pi\sigma D_o$,

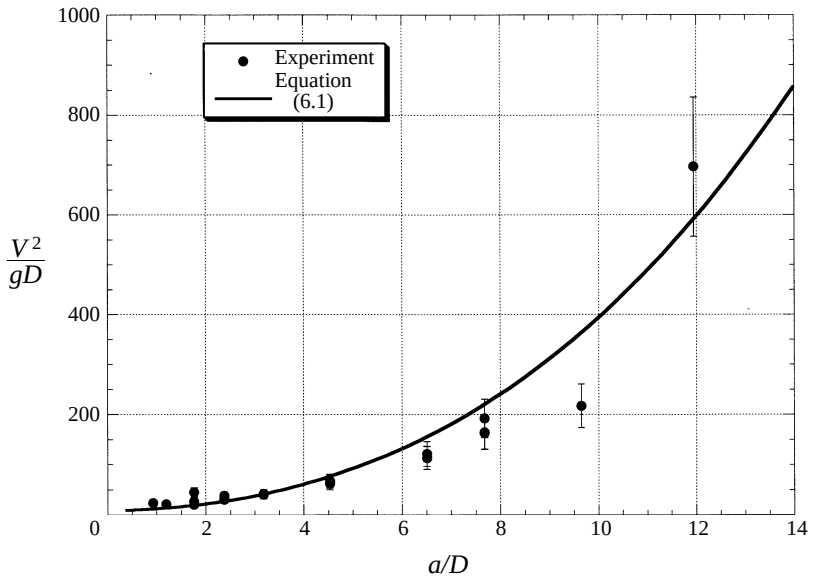

FIGURE 9. Lower velocity threshold of the pulsating mode.

which leads to

$$\frac{V^2}{gD} = \frac{16}{3}\left(\frac{D_o}{D}\right)^3 \left[1 + \tfrac{3}{8}\left(a/D_o\right)^2\right]. \tag{6.1}$$

According to table 2, $0.635 < D_o < 6.1$ mm so that $0.14 < \frac{3}{8}\left(a/D_o\right)^2 < 14$. Surface tension effects are thus dominant for small needles whereas the gravity effect dominates for the bigger ones. The critical value for the Froude number, derived in equation (6.1), is compared to the experimental limits in figure 9. The agreement is within 20%, which is in the range of the experimental accuracy.

Concerning the upper threshold, we distinguish two different mechanisms leading to the end of the oscillations. The first one originates in the capillary instability of the Rayleigh-type undergone by the cylindrical jet. As the height of the fountain is increased, this instability has time to develop so that the jet breaks into droplets prior to reaching the maximum height. When these droplets deviate from the axis a sufficient distance preventing them from interacting with the ascending fluid, the driving cause of the oscillation is lost and the fountain exhibits a quasi-constant height, close to its maximum height H_{max} (figure 1*d*). If the breakup process were symmetric, all the drops would remain on the axis of symmetry and the oscillations would continue independently of the Rayleigh instability. However, the breakup process is not perfect and as they form, the drops acquire a small radial velocity V_y. When they have time to deviate a distance of the order of the jet diameter D before they reach H_{max}, the oscillations stop. Assuming the radial velocity V_y to be proportional to the characteristic velocity V ($V_y \sim \gamma V$ and $\gamma \ll 1$), we define a deviation time, $\tau_{dev} \sim D/V_y$, and compare it to the rising time $T_a \sim V/g$ which is the maximum time allowed for the deviation. To be more precise, we compare T_a to $\tau_{dev} + \tau_R$, where τ_R is the Rayleigh breakup time, $\tau_R \sim 3(\rho D^3/(8\sigma)^{1/2}$. The limit $\tau_R + \tau_{dev} = T_a$ implies

$$\frac{V^2}{gD} \sim \frac{1}{\gamma} + \frac{3}{2}\frac{1}{\gamma^{1/2}}\left(\frac{D}{a}\right). \tag{6.2}$$

D (mm)	D_o (mm)	V_0 (m s^{-1})	Re	V	H_{max}/D
0.495	0.813	1.2	594	1.39	198
0.584	0.902	1.3	759	1.5	196
0.838	1.27	1.5	1257	1.73	182
1.19	1.65	1.9	2261	2.19	206
1.60	2.11	2.1	3360	2.42	187
2.16	2.77	2.7	5832	2.7	172
3.2	4	2.6	8320	2.6	107
4.1	6.1	2.3	9430	2.3	66

TABLE 3. Upper threshold, first mechanism.

D (mm)	D_o (mm)	V (m s^{-1})	K
2.16	2.77	2.7	147
3.2	4	2.6	166
4.1	6.1	2.3	147

TABLE 4. Upper threshold, second mechanism.

According to (6.2), the Froude number should be constant at the upper threshold, in the limit $D/a \ll 1$. Noticing that $H_{max} = V^2/(2g)$, the above relation reduces, in this limit, to $H_{max}/D = 1/(2\gamma)$. Table 3 presents, for each needle, the mean exit velocity at the upper limit, the corresponding Reynolds number, the exit characteristic velocity and finally the critical aspect ratio. In the range $0.495 < D < 1.6$ mm we get that $H_{max}/D = 194 \pm 6\%$. This critical value corresponds to $\gamma \approx 0.25\%$. From table 3, one also may notice that the above criterion does not apply for diameters bigger than 1.6 mm. An additional physical phenomenon affects the stability of the fountain when the dynamic pressure of the jet, $\sim \rho V^2$, becomes of the same order of magnitude as the surface tension restoring action, $\sim 4\sigma/D_p$ (Taylor 1949). In this limit, the lump bursts close to the maximum height and no large-amplitude oscillations are observed. This limit is the one usually observed in public fountains. Using the expression (5.3) for D_p, the threshold is reached for

$$\frac{V^2}{gD} = K\left(\frac{a}{D}\right)^{3/2}. \tag{6.3}$$

The value of K can be evaluated from the experimental values presented in table 4 as $K \approx 153 \pm 10\%$. The three limiting mechanisms just identified define an existence domain for the large-amplitude oscillating fountains. This domain is presented in the plane $\left(a/D,\ V^2/(gD)\right)$ in figure 10 together with the experimental measurements of the oscillations and the experimental limits of existence. Thus, the domain in which the oscillations can be observed extends from $a/D \approx 0.6$ to $a/D \approx 10$, which, for water, corresponds to $D = 6.3$ mm and $D = 0.38$ mm respectively. These limits are in close agreement with our observations, and one should notice that close to these limits, the domain of existence in terms of $V^2/(gD)$ is narrow. It is to be emphasized that these limits depend on the relation $D_o = f(D)$, as already notice in the study of the lower threshold.

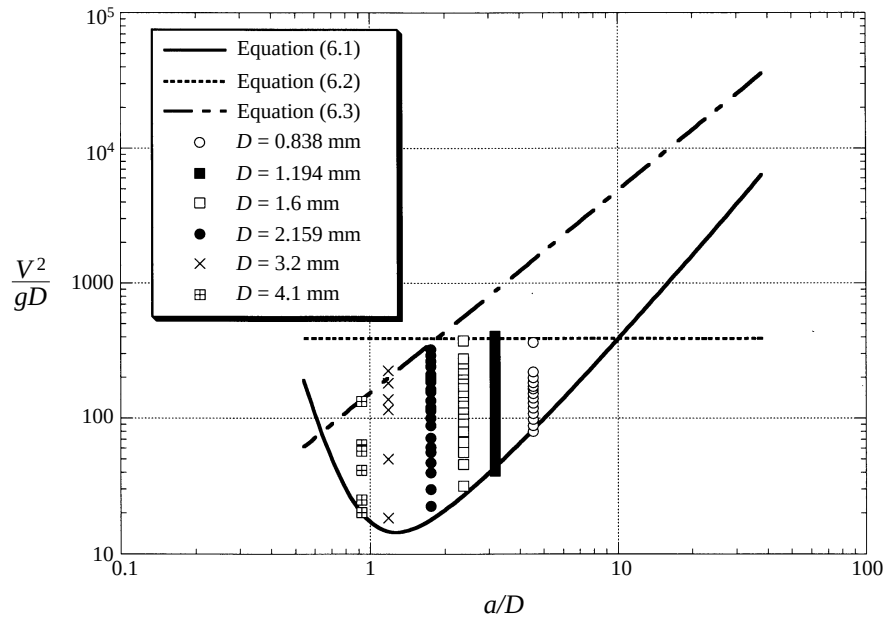

FIGURE 10. Region of existence of the pulsating regime.

7. Conclusion

In a restricted range of Bond and Froude numbers, an upward moving vertical fountain is shown to exhibit large-amplitude pulsations. The frequency of these oscillations is found experimentally to be inversely proportional to the jet's initial velocity, and to be independent of its diameter.

A model based on the interaction of a fluid lump forming at the fountain's tip and the ascending jet is proposed, and shown to be in good agreement with the measured frequencies.

The pulsating mode is shown to be bounded by upper and lower velocity thresholds. The lower limit is determined by the minimum momentum flux needed to overcome gravity and capillary forces. The upper limit results from instabilities, either in the jet or in the lump, leading to the loss of the interaction between the rising and falling fluid.

First, I would like to thank J. C. Lasheras, who gave me the opportunity to work for 16 months at UCSD in his laboratory at the AMES Department. I would also like to thank J. C. Lasheras and E. Villermaux for providing a critical reading of the original version of this paper. Their remarks and suggestions, as well as lots of stimulating discussions, lead to numerous improvements in the final version of the 'manuscript'. This work also results from several discussions with A. Liñán, whose insight in mechanics provided a new dimension to the work. Finally, I would like to thank the US Office of Naval Research which partially supported this work.

Appendix A. Study of the tilted fountain

In order to determine the functional dependency of the maximum fountain height needed in the model of the pulsations, we conducted a parametric study of the stationary trajectories of fountains tilted at an angle θ with the vertical. The measured

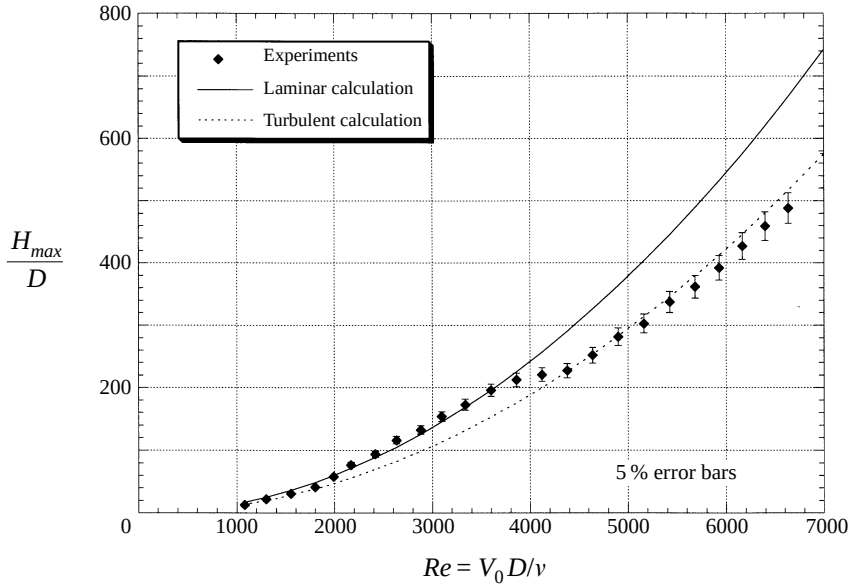

FIGURE 11. Variation of the height as a function of the Reynolds number, $D = 1.6$ mm and $\theta = 15°$.

non-dimensional maximum heights are shown in figure 11, as a function of the jet Reynolds number, $Re \equiv V_0 D/\nu$, for $D = 1.6$ mm and $\theta = 15°$. The experimental measurements show an inflection point at a Reynolds number around 4000. The amplitude of this inflection is well above the experimental error which is estimated at 5%. The variation of momentum of each fluid element is due to the forces acting on it, namely gravity and viscosity. Let us first neglect the viscosity effect. If the initial velocity profile is a top hat type, each fluid element has originally the same momentum MV, and can reach the same maximum height $H_{max} = (V\cos(\theta))^2/(2g)$ after the time T_a, needed for the gravity to reduce this momentum to 0 ($MV \sim MgT_a$). This constitutes the *ballistic* approximation. However, the nozzle we considered exhibits a fully developed pipe flow profile at the exit, which means a parabolic profile in a laminar flow, and a logarithmic one in a turbulent flow (Landau & Lifchitz 1971). The fluid elements do not all have the same momentum at the nozzle's exit and we must take into account the velocity profile to calculate the actual height reached by the jet. This can be done by defining an equivalent jet with a top hat profile that has the same momentum as the original jet. Considering a cylindrical nozzle of diameter D, the radial distance being r, the velocity V of the equivalent jet is related to the actual velocity $v(r)$ by the relation

$$\rho\frac{\pi D^2}{4}V^2 = \rho 2\pi\int_0^{D/2} rv(r)\mathrm{d}r. \tag{A 1}$$

In the laminar case, $v(r) = 2V_0\left[1-\left(2r/D\right)^2\right]$ and the integration of equation (A 1) leads to the relation

$$V = \frac{2}{\sqrt{3}}V_0. \tag{A 2}$$

In the turbulent case, $v(r)/u^* = B + 1/K\ln\left[(D/2-r)u^*/\nu\right]$ where u^* is the friction velocity and K and B two constants whose values can be taken as 0.41 and 5

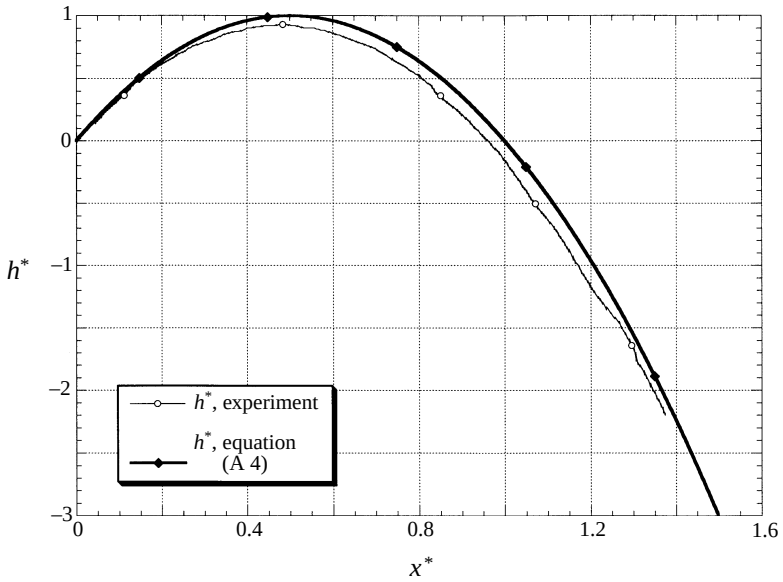

FIGURE 12. Parabola obtained with a laminar tilted fountain, $V_0 = 1.3$ m s^{-1}, $D = 1.6$ mm, and $\theta = 25°$.

respectively. The integration of equation (A 1) leads to the relation

$$V = V_0 \left(1 + \frac{5}{4K^2}\left(\frac{u^*}{V_0}\right)^2\right)^{1/2}. \tag{A 3}$$

The term u^*/V_0 is always small compared to 1 and we can assume that the relation $V = V_0$ holds for a turbulent flow, thus reflecting that the turbulent velocity profile is close to a top hat one.

Using this equivalent jet, we can apply the *ballistic* approximation to obtain two evaluations for the maximum height $H_{max} = V^2/2g$ valid for the laminar and turbulent cases respectively. These two approximations are presented in figure 11. As expected, the laminar calculation agrees very well with the experimental measurements corresponding to the small Reynolds numbers (from 0 to 4000), while the turbulent calculation reproduces large Reynolds number cases ($\geqslant 4000$). The critical value 4000 is only representative of this injector. For the different fountains we used, this threshold value was found to vary from $Re = 2500$ up to $Re = 4000$.

The parabolic nature of the trajectory is presented in figure 12. In this example, $D = 1.6$ mm, $\theta = 25°$ and the mean velocity V_0 is 1.3 m s^{-1}. The vertical and horizontal lengths have been non-dimensionalized by $h^* = h(2g)/(V\cos(\theta))^2$ and $x^* = xg/(V^2\sin(2\theta))$. Since, in this case, the Reynolds number is 2080, we use the laminar value of V ($V = 2/\sqrt{3}V_0 \approx 1.5$ m s^{-1}). The theoretical curve presented in figure 12 corresponds to the parabola obtained with the *ballistic* approximation:

$$h^* = 4x^*(1 - x^*). \tag{A 4}$$

One notices that the two curves are close to each other, the experimental points lying under the theoretical prediction due to the effect of the viscous drag which was neglected. A similar effect of the viscosity was noticed by G. I. Taylor during his study of water-bells (Taylor 1959).

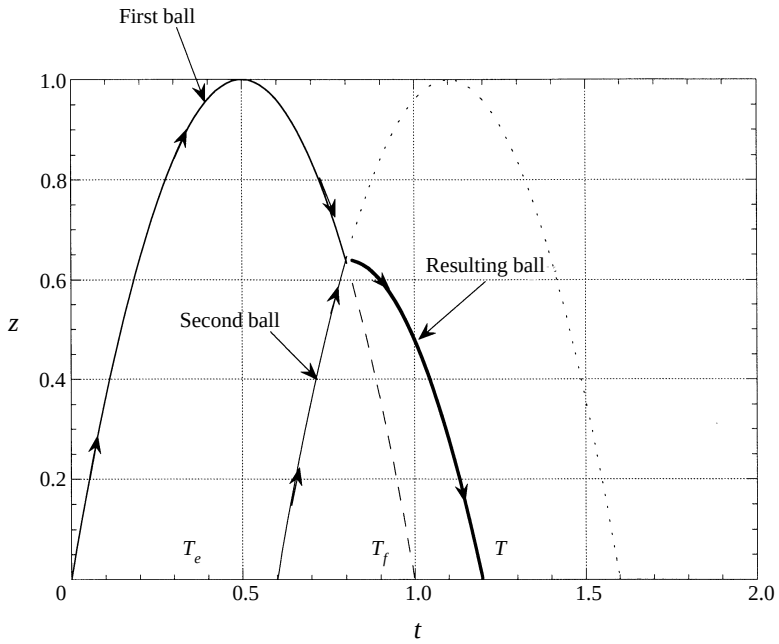

FIGURE 13. Scheme of the juggler problem.

Appendix B. The one-dimensional juggler

We consider here the case of a juggler who throws solid spheres vertically with a constant initial velocity V at a constant period T_e. In the one-dimensional approximation, these balls never deviate from the vertical axis. We assume that all the balls have the same initial mass M, and that each time they collide, they form a new sphere, whose mass and velocity are given by the conservation of mass and momentum. The question is to determine, as a function of T_e, the time T it takes for all the spheres to fall back to their initial position.

If only one ball is thrown by the juggler, this ball reaches its maximum height $H_{max} = V^2/2g$, and then falls back to the origin after the time $T_f = 2V/g$. In the following, both quantities H_{max} and T_f are used to non-dimensionalize length and time. Obviously, if $T_e \geqslant 1$, the time it takes for all the balls to fall back is 1, the individual time of flight. The problem $T_e \leqslant 1$ is more interesting, in the sense that in the limit $T_e \to 0$, it recovers our model of the liquid fountain. The case $T_e = 3/5$, is presented in figure 13. The first ball is released at the time $t = 0$, reaches its maximum $z = 1$ at $t = 1/2$ and interacts with the second ball (emitted at $t = 3/5$) at the time $T_m(1) = 4/5$. This interaction takes place at $Z_m(1) = 16/25$, and the resulting ball falls back to the origin at the time $T = 6/5 > 1$.

The general problem leads, after some calculations, to the following expressions for the time $T_m(n)$ and the location $Z_m(n)$ of the nth collision:

$$T_m(n) = \frac{3 + (4n-1)T_e}{6}, \tag{B 1}$$

$$Z_m(n) = 1 - \left(\frac{2n+1}{3}T_e\right)^2. \tag{B 2}$$

We then consider the family of T_e such that for $n = n^*$ the nth collision takes place

at the origin. The first members of this family are $\left[1, \frac{3}{5}, \frac{3}{7}, \frac{3}{9}, \frac{3}{11}, \ldots\right]$. From equation (B 2), we get that the number of collisions n^* made by the falling ball reaching the origin is related to T_e by the relation

$$n^* = \frac{1}{2}\left(\frac{3}{T_e} - 1\right). \tag{B 3}$$

Using this relation in equation (B 1) leads to the evaluation of the period:

$$T = \tfrac{1}{2}(3 - T_e). \tag{B 4}$$

For $T_e = 1$, we recover $T = 1$ and in the limit $T_e \to 0$, the period tends to $3/2$, which is the same limit as the one obtained with the continuous model presented in § 4.

REFERENCES

Dias, F. & Vanden-Broeck, J. M. 1990 Flows emerging from a nozzle and falling under gravity. *J. Fluid Mech.* **213**, 465–477.

Landau, L. & Lifchitz, E. 1971 *Physique Theorique: Mecanique des fluides.* Mir.

Priestley, C. H. B. 1953 Buoyant motion in a turbulent environment. *Austral. J. Phys.* **6**, 279–290.

Schulkes, R. M. S. M. 1993 The evolution of capillary fountains. *J. Fluid Mech.* **261**, 223–252

Taylor, G. I. 1949 The shape and acceleration of a drop in a high-speed air stream. *Advisory Counc. on Sci. Res. Tech. Dev.* (Reprinted in Scientific Papers, vol. III, p. 457, Cambridge University Press, 1963.)

Taylor, G. I. 1959 The dynamics of thin sheets of fluid. I water bells. *Proc. R. Soc. Lond.* A **253** 289–295.

Turner, J. S. 1966 Jets and plumes with negative or reversing buoyancy. *J. Fluid Mech.* **26** 779–792.

Villermaux, E. 1994 Pulsed dynamics of fountains. *Nature* **371**, 24–25.

Villermaux, E. & Hopfinger, E. J. 1993 Periodically arranged co-flowing jets. *J. Fluid Mech.* **263**, 63–92.